Passivation Behavior of a Zr60Cu20Ni8Al7Hf3Ti2 Bulk Metallic Glass in Sulfuric Acid Solutions

Junlei Tang[1,2], Yingying Wang [1,], Qiuhong Zhu[1], Mohamad Chamas[1], Hu Wang[3], Jichao Qiao[4], Yuanqiang Zhu[1] and Bernard Normand [5]*

[1] College of Chemistry and Chemical Engineering, Southwest Petroleum University, Chengdu 610500, China;
[2] State Key Laboratory of Oil and Gas Reservoir Geology and Exploitation, Southwest Petroleum University, Chengdu 610500, China;
[3] College of Material Science and Engineering, Southwest Petroleum University, Chengdu 610500, China;
[4] School of Mechanics, Civil Engineering and Architecture, Northwestern Polytechnical University, Xi'an 710072, China;
[5] Université de Lyon, INSA de Lyon, MATEIS CNRS UMR 5510, Villeurbanne 69621, France;
[*]E-mail: yingyingwanglyon@126.com

The passivation behavior of $Zr_{60}Cu_{20}Ni_8Al_7Hf_3Ti_2$ bulk metallic glass (BMG) in H_2SO_4 solutions were studied by electrochemical measurements and X-ray photoelectron spectroscopy. The influence of H_2SO_4 solutions concentration and temperature, heat treatment temperature and erosion on passivation behavior were analyzed. The corrosion resistance of $Zr_{60}Cu_{20}Ni_8Al_7Hf_3Ti_2$ bulk metallic glass decreases slightly with the increase of concentration and temperature of H_2SO_4 solutions. The Zr-based BMG exhibits excellent passivation ability in various H_2SO_4 solutions. The formed passive films in H_2SO_4 solutions possess the semiconductor characteristics depending of applied potential, and show n-type semiconductor in stable passivation region. The main component of passive films is ZrO_2 in competition with HfO_2 and Al_2O_3, and no Ni element, and the alloy surface whose passive film contains less Cu and more Al_2O_3 and less Cu, hence the alloy exhibits can have better corrosion resistance. Annealing which temperatures are lower than T_g were conducted. After the heat treatment, Zr-based BMG maintains amorphous structure, and the electrochemical behavior of Zr-based BMG does not show obvious difference. However, the heat treatment improves BMG' micro-hardness. Consequently, the Zr-based BMG after heat treatment has stronger erosion-corrosion resistance than the as-cast BGM.

1. INTRODUCTION

Bulk metallic glasses (BMGs) have attracted increasing attention due to their distinctive structure and the freedom from defects in traditional metal materials, such as dislocation, grain boundary and second-phase precipitates [1]. It is believed that they have enormous potential for advanced engineering materials [2,3]. Thus plenty of BMGs with high glass-forming ability have been prepared by adopting copper mold casting, water-quenching and suction-casting methods [4].

Usually, corrosion resistance plays an important role in whether the BMGs can be widely applied. The corrosion behavior of BMGs, such as Zr- [5,6], Fe- [7], Mg- [8], Cu- [9], and Ti-based [10] BMGs, has been substantially examined. Among these BMGs, Zr-based metallic glass systems have been specifically investigated since they possess high glass-forming ability, high mechanical strength, excellent process ability and superior corrosion resistance, as exemplified by Zr-Cu [11], Zr-Al-Fe [12], and Zr-Ni-Cu-Al-Y [13] BMGs, etc. Zr-based BMGs exhibit excellent corrosion resistance due to their spontaneous and homogeneous passivation in various aggressive solutions [14,15]. The formed passive films are capable of preventing the aggressive ions approaching the alloy substrate and reducing the corrosion degree. The enrichment of Zr and Al elements in alloys has a significant contribution to the high corrosion resistance of alloys [16]. Nevertheless, the enrichment of Cu element usually accelerates the dissolution or pitting corrosion of the alloy substrate results from the galvanic cell (consisting of Zr and Cu elements) formation [17].

To enhance the corrosion resistance, one or two elements are often added to a certain kind of metallic glass. Some investigations have proposed that ZrCuNiAlM (M = Ti, Hf) BMGs possess the ability of passivation. Dhawan [18] showed that the passivation current density of $Zr_{65}Cu_{17.5}Ni_{10}Al_{7.5}$ amorphous alloy is approximately 3×10^{-4} A·cm^{-2} in 0.5 mol/L H_2SO_4 solution and the passivation current density of $Zr_{59}Ti_3Cu_{20}Al_{10}Ni_8$ amorphous alloy is approximately 3×10^{-6} A·cm^{-2} in 0.5 mol/L H_2SO_4 solution [19], which indicates that the addition of Ti element can improve the corrosion resistance of amorphous alloys. Liu [20] showed that the corrosion resistance of the $Zr_{64}Cu_{17.5}Ni_{10}Al_{7.5}Hf$ amorphous alloy exceeded that of $Zr_{65}Cu_{17.5}Ni_{10}Al_{7.5}$ in NaCl, H_2SO_4, and HCl solutions. Thus, it seems that Hf can also increase the corrosion resistance of amorphous alloys. However, the corrosion effects of adding Ti and Hf together into BMGs have not yet been mentioned in the literatures.

In this study, we examined the corrosion behavior of a Zr-based BMG with the addition of Ti and Hf elements. This $Zr_{60}Cu_{20}Ni_8Al_7Hf_3Ti_2$ BMG showed good mechanical properties [33]. However, up to now, there is no report on its corrosion performance and the properties of its passive film. Therefore, the corrosion and passivation behavior of $Zr_{60}Cu_{20}Ni_8Al_7Hf_3Ti_2$ BMG in various H_2SO_4 solutions and its influence factors were discussed by means of electrochemical methods and surface analysis spectroscopy in this paper.

2. EXPERIMENTAL

The multi-component $Zr_{60}Cu_{20}Ni_8Al_7Hf_3Ti_2$ BMG ingots were prepared by arc melting a mixture of pure Zr, Cu, Ni, Al, Hf and Ti metals (purity > 99.99%) in a Ti-gettered argon atmosphere. Bulk metallic glasses in the plate form with a dimension of 5 mm×2 mm×40 mm was produced by

copper mold casting [34]. The structure of the as-cast sample was examined by X-ray diffraction (XRD) with a X Pert PRO MPD diffractometer equipped with Cu Kα radiation (λ=0.1542 nm).

Prior to electrochemical measurements, the specimens were mechanically ground with 5000# abrasive grit SiC papers, degreased in acetone and then ethanol, rinsed with distilled water, and dried by a cold air drier.

To understand the corrosion mechanism and influence of concentration and temperature of electrolytes for Zr-based BMG, the electrolytes used were 0.0100, 0.1000, and 0.9802 mol·dm^{-3} H$_2$SO$_4$ solutions at 20 ℃ and 0.0100 mol·dm^{-3} H$_2$SO$_4$ solutions at 40 ℃ and 60 ℃, and the electrolytes were prepared from reagent grade chemical and distilled water. Electrochemical measurements were conducted in H$_2$SO$_4$ solutions open to the air, and fresh sulfuric acid solution was used in each experiment. The dried samples connected to a copper wire were coated with silicon resin, leaving an exposed working area of 0.5 mm^2. The electrochemical measurements were carried out in a three-electrode cell by using a platinum counter electrode and a Hg$_2$/Hg$_2$SO$_4$ reference electrode (MMSE, E$_{MMSE}$ = -0.615 V$_{SHE}$). All electrochemical measurements were conducted by using the CHI660E electrochemical measurement system. Prior to performing each experiment, the working electrode was cathodic polarized at -1.5 V for 1000 s to remove the natural oxide film.

Potentiodynamic polarization curves were obtained with a potential sweep rate of 0.5 mV/s and began at -0.7 to 1.3 V$_{MMSE}$. Electrochemical impedance spectroscopy (EIS) was performed at an AC amplitude of 10 mV and in the frequency range of 100 kHz to 10 mHz. EIS data were fitted by using ZSimpWin software. The Mott-Schottky tests were performed with a sweep rate of 10 mV at the frequency of 1000 Hz with the same range potential as potentiodynamic polarization.

The erosion-corrosion tests were performed in a 0.0100 mol·dm^{-3} H$_2$SO$_4$ solution at 25 ℃ with SiO$_2$ particles. The average size of SiO$_2$ used in this work was approximately 100 mesh (149 μm). The erosion-corrosion behavior of Zr$_{60}$Cu$_{20}$Ni$_8$Al$_7$Hf$_3$Ti$_2$ was conducted in a rotating device consisting of a water-bath, a glass cell, an agitator and the electrochemical system, as shown in Fig. 1. The mixing arm was located at the center of the glass cell, and the working electrode was approximately 0.5 mm^2. The angle between the sample and the cell wall was set to 30º, and the stirring speed was set to 1000 r/min (2.09 m/s). The concentration of SiO$_2$ particles was 13.33 g/L. The electrochemical tests referred to the above.
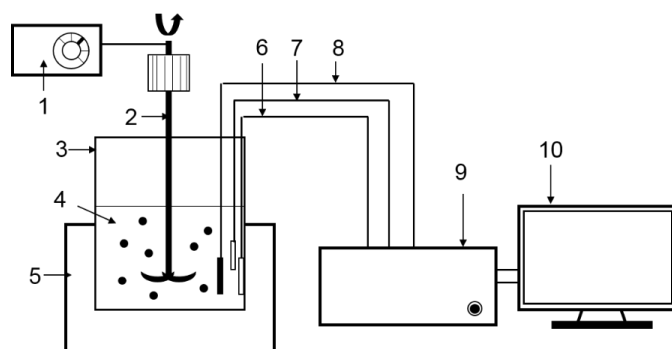

Figure 1. Schematic diagram of the erosion-corrosion test device: 1. rotator, 2. speedometer, 3. vessel, 4. test solution, 5. water-bath, 6. working electrode, 7. reference electrode, 8. counter electrode, 9. electrochemical workstation, 10. computer.

The surface analysis was conducted with X-ray photoelectron spectroscopy (XPS), after immersing in a 0.0100 mol·dm^{-3} sulfuric acid solution at 20 ℃ for 8 hours. The XPS measurement was conducted by using an ESCALAB 250 photoelectron spectrometer with Al-kα radiation (hν = 1486.6 eV). The binding energies of Zr, Cu, Ni, Al, Hf, Ti, and O were from the XPS database "www.lasurface.com." The peak-fit processing was conducted using XPSPEAK4.1 software, and the deconvolution of peaks used Newton's iteration method.

3. RESULTS AND DISCUSSION

3.1. Material structure characterization

Fig. 2 shows the X-ray diffraction patterns of $Zr_{60}Cu_{20}Ni_8Al_7Hf_3Ti_2$ BMGs in different states. The pattern of as-cast sample exhibits a typical broad peak at a 2θ angle located between 32º to 40º, and a second broad peak at a 2θ angle = 65º. After heat treatments at 500 K and 600 K, the samples maintain the amorphous structure.
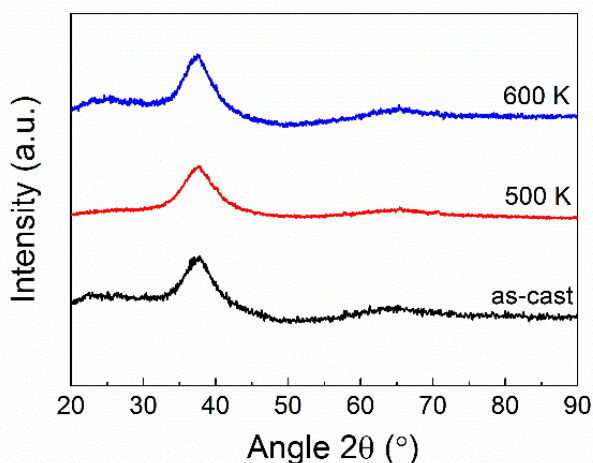

Figure 2. XRD patterns of as-cast Zr-based BMG and BMGs with different heat treatments.

3.2 Influence of H_2SO_4 solution concentration on passivation behavior

3.2.1. Electrochemical measurements

Fig. 3 shows the potentiodynamic polarization curves for Zr-based BMG in different concentrations of H_2SO_4 solutions. All of the curves have very close corrosion potentials and two passivation zones. It reveals that the alloy has similar corrosion behavior in various sulfuric acid solutions. According to the features of zone I and zone II, the $Zr_{60}Cu_{20}Ni_8Al_7Hf_3Ti_2$ BMG possesses two passivation regions in all H_2SO_4 solutions at 20 ℃.
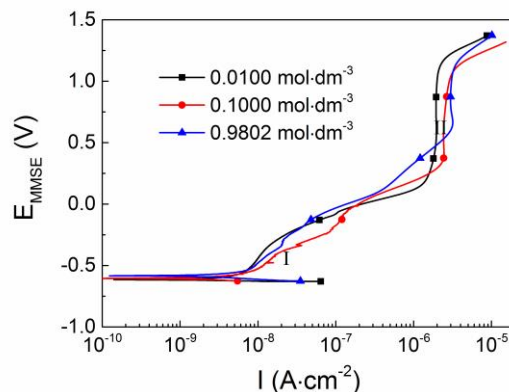
Figure 3. Potentiodynamic polarization curves of Zr-based BMG in different concentration H_2SO_4 solutions open to air.

Table 1. Parameters of potentiodynamic polarization curves.

| H_2SO_4 ($mol\cdot dm^{-3}$)	E_{corr} (V)	$i_{corr}\times10^9$ ($A\cdot cm^{-2}$)	$i_p\times10^6$ ($A\cdot cm^{-2}$)	ΔE (V)
0.0100	-0.616	2.208	1.930	0.998
0.1000	-0.605	3.170	2.498	0.733
0.9802	-0.583	4.887	3.100	0.515

The relevant parameters of the polarization curves are summarized in Table 1, including corrosion potential (E_{corr}), corrosion current density (i_{corr}), passive current density (i_p) and the width of passivation region (ΔE). ΔE represents the width of the second passivation region and the passive current density (i_p) is read from the second passivation region at 0.75 V. At the same time, i_{corr} is also present, which is calculated by Tafel fitting [21]. It is clear that i_{corr} increases and ΔE decreases with the increase of acid concentration, which suggests that the corrosion rate and the width of second passivation are sensitive to solution concentration. However, the transpassive potential only changes slightly with variation in the concentration because the transpassivation of the passive films mainly relies on the oxygen concentration and applied potential other than the H^+ concentration in sulfuric acid. Similar passivation behavior is investigated on In-718 alloy in acidic solutions [22].

As beneficial elements to surface passivation, Hf and Ti are normally used to enhance the passivation ability of traditional alloys, for instance, stainless steels [23]. In the cases of Zr-based BMGs, the i_p of $Zr_{60}Cu_{20}Ni_8Al_7Hf_3Ti_2$ BMG in a 0.9802 $mol\cdot dm^{-3}$ H_2SO_4 solution is almost the same as that of $Zr_{59}Ti_3Cu_{20}Al_{10}Ni_8$ BMG in a 0.5 $mol\cdot dm^{-3}$ H_2SO_4 solution; the i_{corr} of $Zr_{59}Ti_3Cu_{20}Al_{10}Ni_8$ BMG is larger than that of $Zr_{60}Cu_{20}Ni_8Al_7Hf_3Ti_2$[19]. Both results indicate that the addition of Hf element can improve the corrosion resistance of ZrTiCuAlNi series BMGs. Compared with the electrochemical properties of $Zr_{65-x}Hf_xCu_{17.5}Ni_{10}Al_{7.5}$ BMG in 0.5 $mol\cdot dm^{-3}$ H_2SO_4 solution [20], i_p and i_{corr} of $Zr_{60}Cu_{20}Ni_8Al_7Hf_3Ti_2$ in 1 M H_2SO_4 solution present lower values [19], indicating that the addition of Ti can also benefit the corrosion resistance of BMGs. Moreover, $Zr_{60}Cu_{20}Ni_8Al_7Hf_3Ti_2$ BMG exhibits two passivation potential regions in different concentrations of H_2SO_4 solutions. The

first one is above the corrosion potential with a very low anodic current density of approximately 10^{-9} to 10^{-8} orders of magnitude. Another is above 0.2 V with a passive current density of 10^{-6} orders of magnitude. This phenomenon can be attributed to the contribution from both titanium and hafnium.

The EIS results of the sample in different concentrations of H_2SO_4 solutions open to air are presented in Fig. 4. From the plots of Nyquist vs. time in Fig. 4a, stable passive films can be formed on the surface of the BMG alloy within 4 hours in H_2SO_4 solutions with various concentrations. Fig. 4a shows that all plots have an unfinished capacitance arc with high impendence values of 10^5 to 10^6 orders of magnitude, indicating very good corrosion resistances. The capacitance loops of the sample in a 0.9802 mol·dm^{-3} H_2SO_4 solution are always the smallest and narrow down a little with time evolution, indicating that the corrosion resistance of passive films in that solution is not as good as in other solutions. Fig. 4b and Fig. 4c present the Bode plots at the 24th hour in acid solutions with various concentrations. The Bode-phase plots show one probable time constant, and the phase angles in the low-frequency region are close to - 90º, which indicates the formation of stable and protective passive films on the surface of the alloy in H_2SO_4 solutions.
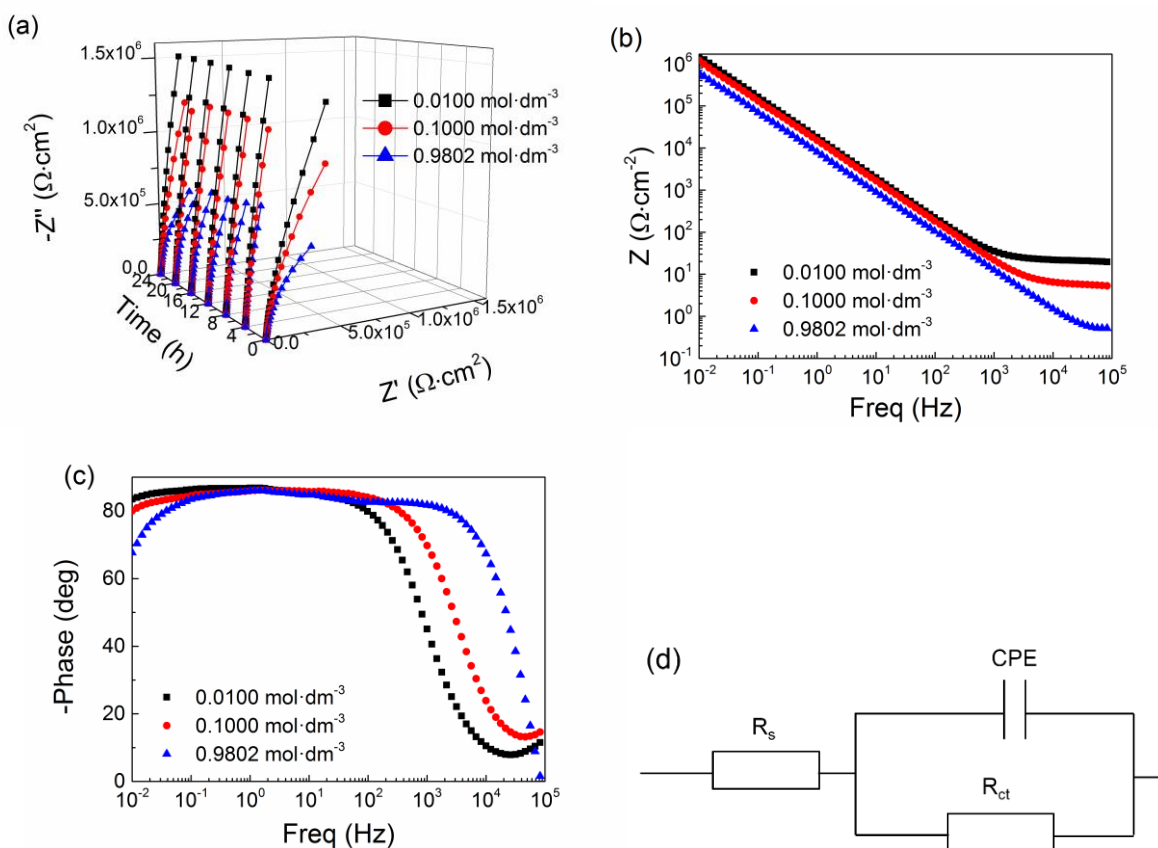
Figure 4. EIS of Zr-based amorphous at OCP in different concentration H_2SO_4 solutions open to air, (a) Nyquist plots, (b) log Z plots at 24th hours, (c) Bode phase angle at 24th hours (d) the equivalent electric circuit used to fit the EIS spectra.

The equivalent circuit as shown in Fig. 4d is chosen for fitting the EIS spectra according to the above observation, which was used in the case of Nyquist plots exhibiting only one simple capacitive

semicircle with a large radius and the phase Bode plots exhibiting a line near - 90º in the middle-frequency region. It consists of the solution resistance (R_s), the charge-transfer resistance (R_{ct}), and the capacitance of a constant phase element (CPE) representing the protective layer (passive films). Fig. 5 displays the R_{ct} plots with time variation, which the evolution tendency of R_{ct} can be seen. The slope decreases with the increase in solution concentration, and the plots illustrate that the formation of passive films is easier and faster in lower concentration H_2SO_4 solutions. It is clear in Fig. 5 that the passive films develop fleetingly within the first 4 hours under all conditions; however, the growth rate of passive films is mitigated under higher concentrations and in later time.
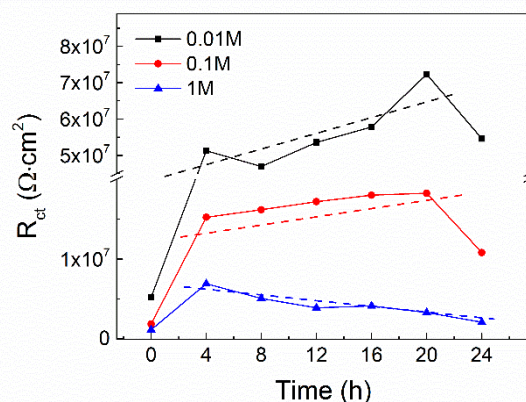

Figure 5. R_{ct} vs. time correlative curves of Zr-based amorphous at OCP in different concentration H_2SO_4 open to air.

3.2.2. XPS analysis

To obtain the chemical composition of passive films and elucidate the corrosion resistance mechanism of alloy in H_2SO_4 solutions, XPS analysis was performed for one sample that was immersed for 8 hours in a 0.0100 mol·dm^{-3} H_2SO_4 solution at 20 ℃. All of the high-resolution scanning XPS spectra of the detected peaks except C 1s are shown in Fig. 6. The C 1s peak with a binding energy of 284.8 eV was due to contaminant carbon on the specimen surface and contributed to the calibration of the binding energies of other elements. The Zr 3d spectra consist of two peaks with multiplet splitting, $3d_{5/2}$ and $3d_{3/2}$, which can be regarded as the oxide states of Zr element (Fig. 6a). The peaks at 181.92 eV and 184.3 eV, respectively, correspond to $3d_{5/2}$ and $3d_{3/2}$ splitting orbits of Zr^{4+}. The peak at 73.68 eV corresponds to Al^{3+}. The Al 2p spectra are overlapped by the Cu 3p spectra, as shown in Fig. 6b, the main peak at 73.5 eV is from Al_2O_3 and the wide peak of Cu 3p consists of two splitting peaks, which located at 75.7 eV and 77.5 eV, respectively. Peaks at 932.19 eV and 952.04 eV can be assigned to Cu $2p_{3/2}$ and $2p_{5/2}$, respectively, as shown in Fig. 6c. Both of these two peaks have two doublets; the main ones are from metallic copper, and the other two with higher binding energies are from CuO.
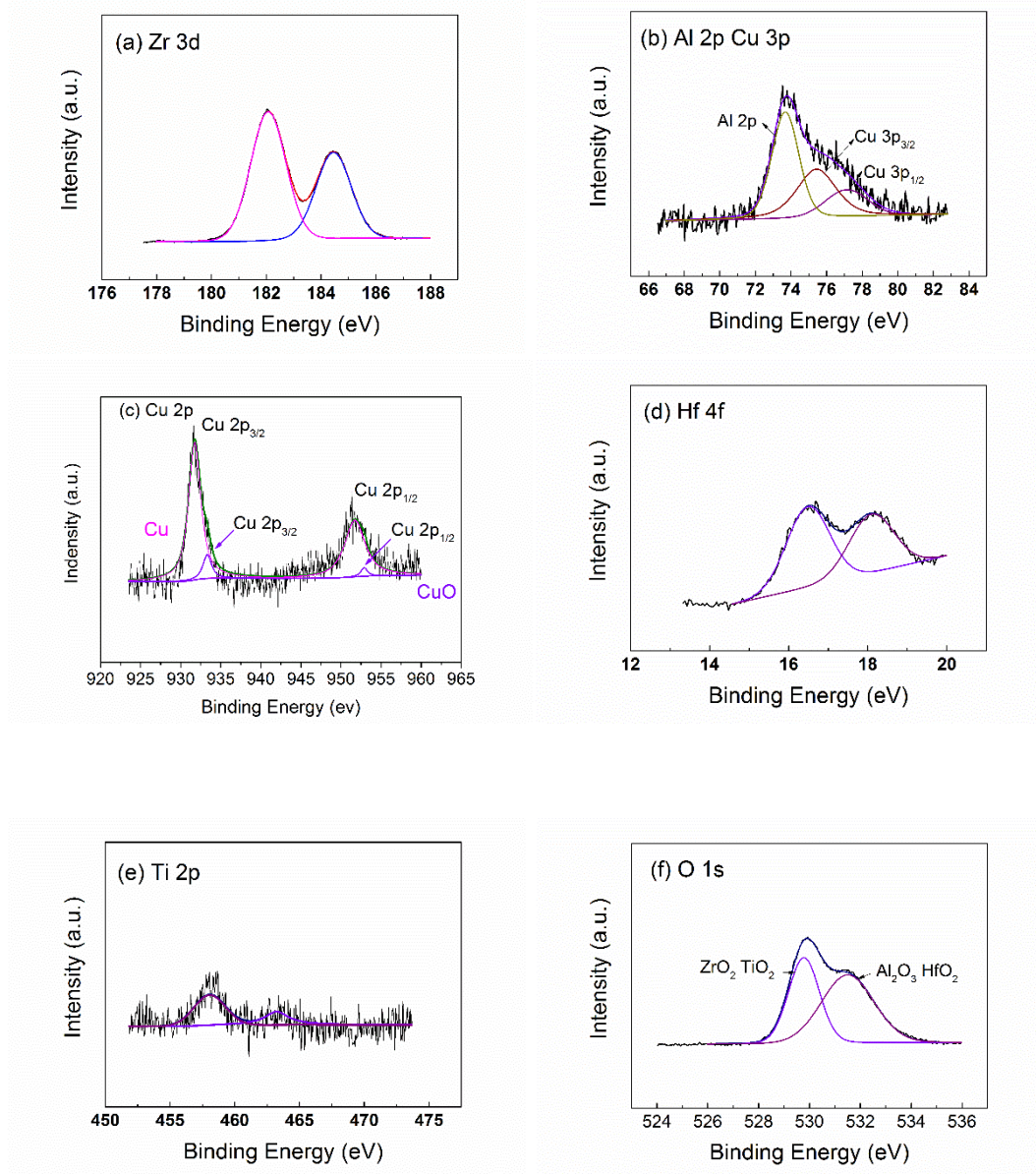
Figure 6. XPS spectra of Zr-based BMG after polarization at 0.5 V for 0.5 hours and immersing for 8 hours in 0.0100 mol·dm^{-3} H$_2$SO$_4$ solution open to the air at 20 °C.

Fig. 6d shows that the peaks of 17.84 eV and 16.31 eV are assigned to Hf 4f from Hf^{4+}. The Ti 2p spectra consist of a set of 2p$_{3/2}$ and 2p$_{1/2}$ peaks of the oxide state, as shown in Fig. 6e. The peaks of 463.18 eV and 458.12 eV are assigned to Ti 2p$_{3/2}$ and Ti 2p$_{1/2}$, respectively, from Ti^{4+}. Fig. 6f shows that the O 1s spectra are composed of multifarious overlapping peaks from 527 eV to 535 eV, which are assigned to Oxygen-Metal (OM) oxygen and OH oxygen. The OM oxygen signifies oxygen with a metal-oxygen bond and corresponds to the O^{2-} ions of oxide, mainly ZrO$_2$ and Al$_2$O$_3$. The OH oxygen is oxygen in bound water in the surface films.

Table 2 summarizes the atomic concentration of passive films formed after immersion for 8 hours in a 0.0100 mol·dm^{-3} H$_2$SO$_4$ solution at 20 ℃. It is obvious that the passive films are enriched with Zr and Al metallic elements, Cu is deficient with respect to the nominal alloy compositions, and

the Ni spectrum is not detected. According to the above results, it can be concluded that the main composition of the passive films is ZrO_2 and Al_2O_3, which also contain a small quantity of TiO_2, HfO_4, Cu and CuO.

When the specimen is immersed in the H_2SO_4 solution for 8 hours, Cu and Ni elements are preferentially dissolved in solution, which leads to the enrichment of Zr, Al and other passivable elements on the surface. Numerous studies show that ZrO_2 [24,25] and Al_2O_3 [26,27] films can improve the corrosion resistance of materials. The $Zr_{60}Cu_{20}Ni_8Al_7Hf_3Ti_2$ BMG possesses high corrosion resistance can be attributed to the enrichment of Zr and Al on the surface of the alloy, which is able to insulate the alloy substrate from the aggressive solutions by forming stable and compact oxides.

The presence of small amounts of Hf and Ti on the surface also enhances passivation stability due to the formation of Hf^{4+} and Ti^{4+} oxides according to the XPS analysis. It seems that Hf has more contribution to the passivation than Ti due to its higher content in the passive film and by comparing the corrosion performance of $Zr_{60}Cu_{20}Ni_8Al_7Hf_3Ti_2$ BMG with that of $Zr_{59}Ti_3Cu_{20}Al_{10}Ni_8$ [19] and $Zr_{65-x}Hf_xCu_{17.5}Ni_{10}Al_{7.5}$[20]. From the observation of the element ratio before and after the passive film formation in each condition (Table. 2), Hf has an advantage in competing with other elements, except for Al, in the BMG alloy to form a stable oxide in the passive film. The competition ability follows the order of Al, Hf, Ti and Zr.

Table 2. Compositions of the surface films for the amorphous alloy after polarizing at 0.5 V for 0.5 hours and immersing for 8 hours in a 0.0100 mol·dm^{-3} H_2SO_4 solution open to air at 20 ℃.

Zr-Based alloy	Zr	Cu	Ni	Al	Hf	Ti	O
As-cast (nominal)	60	20	8	7	3	2	0
Immersed for 8 h	24.64	1.01	0	15.76	1.65	0.70	56.24
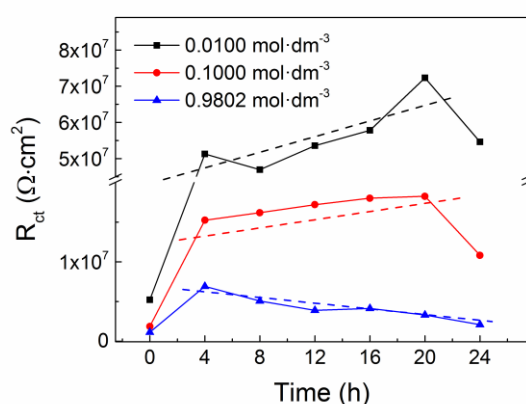
Figure 7. Mott-Schottky curves of formed passive films of the Zr-based BMG at OCP in different concentration H_2SO_4 solutions open to air.

3.2.3. Mott-Schottky curve analysis

It is recognized that the passive films of alloys consist of one or several oxides and their thickness range is from several nanometers to tens of nanometers, possessing typical semiconductor properties. Consequently, in order to obtain more information about the properties of passive films, the Mott-Schottky curves were obtained. The properties of the formed passive films of samples in various sulfuric acid solutions were characterized by the following equation:

$$Q = -sin\left(n\frac{\pi}{2}\right)\frac{1}{(2\pi f)^n Z_j} \qquad (1)$$

where n is the exponent of the CPE, and the value of n was obtained from EIS measurement at 8 hours. f is the frequency (1000 Hz) and Z_j is the measured imaginary impedance. The value of C in equation 2 is calculated by equation 1.

$$\frac{1}{C^2} = \frac{2}{\varepsilon\varepsilon_0 eN}\left(E - E_{fb} - \frac{kT}{e}\right) \qquad (2)$$

where ε_0 is the permittivity of free space (8.854×10^{-14} F·cm^{-1}), ε is the dielectric of the passive films, E is the applied potential, E_{fb} is the flat band potential, k is the Boltzmann constant (1.38×10^{-23} J·K^{-1}), T is the absolute temperature, e is the electron charge (1.6×10^{-19} C), and N is the donor density in an n-type passive film or acceptor density in a p-type passive film.

The capacitance of the space-charge region of the passive films as a function of potential ($1/Q^2$ - E curves) is used to determine the semiconductor property of the passive films, and a positive slope of the curve indicates an n-type semiconductive property of the passive films whereas a negative slope indicates p-type. Fig. 7 shows the Mott-Schottky curves for the passive films formed in the H_2SO_4 solutions. ε is taken as 12.5, and the value of kT/e can be ignored. The calculated acceptor (donor) densities (N_A (N_D)) for the passive films formed on Zr-based BMG are shown in Table 3 in various H_2SO_4 solutions.

Table 3. Mott-Schottky parameters of passive films on Zr-based BMGs

H$_2$SO$_4$ (mol·dm^{-3})	n-Type (-0.6;-0.35 V)		p-Type (-0.2;0.2 V)		n-Type (0.3;0.9 V)	
	N$_D$(cm^{-3})×10^{-21}	E$_{fb}$ (V)	N$_A$(cm^{-3})×10^{-21}	E$_{fb}$ (V)	N$_D$(cm^{-3})×10^{-21}	E$_{fb}$ (V)
0.0100	2.25	-4.8	3.10	5.5	0.75	-1.2
0.1000	3.37	-4.3	4.26	4.9	1.30	-1.0
0.9802	4.54	-4.4	5.49	4.4	1.34	-0.8

It is observed that the semiconductor type of the passive films depends on the applied potential. As shown in Fig. 7, three regions of potential are observed: from -0.6 to -0.35 V, from -0.2 to 0.2 V and from 0.3 to 0.9 V, which are named regions M1, M2 and M3, respectively, indicating the existence of multiple oxides in the passive films. In region M1, the Mott-Schottky curves show positive slopes in the negative applied potential, which exhibit n-type semiconductor behavior in the accumulation of charge carrier (electron to the solution) due to the formation of the passive film. The slopes are negative and the passive films exhibit p-type semiconductor depletion (the potential is towards the positive in region M2). These electrons will be taken from the solution in the reaction with the surface

of the electrode. The slopes are positive and the passive films exhibit n-type semiconductor behavior in the M3 region. The slopes of the Mott-Schottky curves are obviously susceptible to the concentration and decrease with increasing concentration. Table 3 implies that N_A and N_D of the passive films increase when the passive films are formed in higher concentration acid solutions, indicating that a higher concentration causes the formed passive films to have a higher impurity density.

The flat band potentials (E_{fb}) are very close in different solutions, indicating the formation of the same passive layer on the surface of Zr-based BMG. Nevertheless, the high value of the flat band potential is due to the formation of a stable dielectric layer. All slopes are parallel, which indicates the influence of the band-edge [28]. Exceeding 0.9 V, the passive films emerge as a p-type semiconductor, which is probably caused by the low-valence oxide being oxidized to a high-valence oxide or transformed into hydroxide.

J. Bisquert *et al.* calculated the Helmholtz capacitance for $SnO_2(F)$/solution interface/TiO_2 by comparing different electrodes and corrected the apparent flat band potential due to the effect of band unpinning [29]. H.J. Jang *et al.* conducted photoelectrochemical analysis of passive films formed on Ni, and its alloys demonstrated a p-type semiconductor property in the formed passive films [30]. They calculated that the flat band potential of the passive film on Ni was 0.3 V_{SCE}, while that of the thermal oxide was 0 V_{SCE}. They demonstrated that the capacitance of the passive films appeared to be dominated by that of the outer hydroxide layer $Ni(OH)_2$.

Z. Petrovic *et al.* carried out Mott-Schottky analysis and demonstrated that the depletion region in the passive films close to the film/electrolyte interface dominated the semiconducting properties [31]. They showed that the passive films on Cr in an acid solution behaved as an n-type semiconductor and gave an energy-band structure model of the passive films with E_{fb} value equal to -0.83 V(vs. Ag/AgCl), corresponding to the passive films inside the potential region of 0.40 -0.80 V(vs. Ag/AgCl).

From the discussion above, we can conclude that the passive films of $Zr_{60}Cu_{20}Ni_8Al_7Hf_3Ti_2$ BMG show n-type semiconductor behavior and the composition of the passive films is ZrO_2, Al_2O_3, and HfO_2 (n-type semiconductor behavior in sulfuric solution) by XPS; no NiO or $Ni(OH)_2$ (p-type) is found. The formed passive films on the surface of Zr-based BMG possess identical components in H_2SO_4 solutions open to the air.

3.3 Influence of H₂SO₄ solution temperature on passivation behavior

Fig. 8 shows the potentiodynamic polarization curves for Zr-based BMG in different temperature H_2SO_4 solutions open to air. Table 4 reveals the parameters of potentiodynamic polarization. The potentiodynamic polarization shows a passivation zone and the transpassivation potential decreases when the temperature increases. Moreover, the transpassivation potential is lower at higher temperatures because of the decrease in the oxygen concentration. Results also reveal that the temperature has an apparent effect on the corrosion behavior of $Zr_{60}Cu_{20}Ni_8Al_7Hf_3Ti_2$ BMG. The increase in temperature weakens the passivation ability of the sample as the anodic current density increases with the temperature. However, ΔE only decreases slightly while i_p increases and E_{corr} shows

no obvious change. The above phenomenon indicates that the corrosion resistance of the BMG alloy does degrade with the increase of temperature, but it is more susceptible to sulfuric acid concentration.
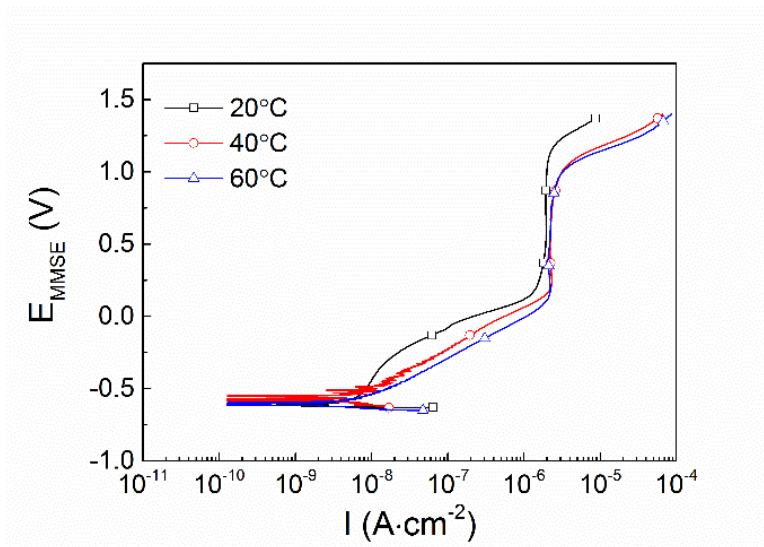

Figure 8. Potentiodynamic polarization curves of Zr-based BMG in different temperature H_2SO_4 solutions open to air.

**Table 4.** Parameters of potentiodynamic polarization curves.

T (℃)	E_{corr} (V)	$i_{corr} \times 10^9$ (A·cm^{-2})	$i_p \times 10^6$ (A·cm^{-2})	ΔE (V)
20	-0.616	2.208	1.93	0.998
40	-0.587	4.786	2.203	0.826
60	-0.599	4.966	2.223	0.846

Fig. 9a shows the plots of Nyquist vs. time with solutions at different temperatures. Stable passive films can be formed on the surface of the BMG alloy within 4 hours in H_2SO_4 solutions with various temperatures. Fig. 9b and Fig. 9c present the Bode plots at the 24th hour in acid solutions with various temperatures. The Bode-phase plots show one probable time constant, and the phase angles in the low-frequency region are close to -90º, which indicates the formation of stable and protective passive films on the surface of the alloy in H_2SO_4 solutions.

The equivalent circuit as shown in Fig. 4d is also chosen to fit the EIS spectra with solutions at different temperatures. Fig. 10 displays the R_{ct} plots with time variation, from which the evolution tendency of R_{ct} can be seen. It can be observed in Fig. 10 that the passive films develop fleetingly within the first 4 hours under various temperature conditions, which is similar to various concentration conditions; however, the growth rate of the passive films decreases with higher temperature.
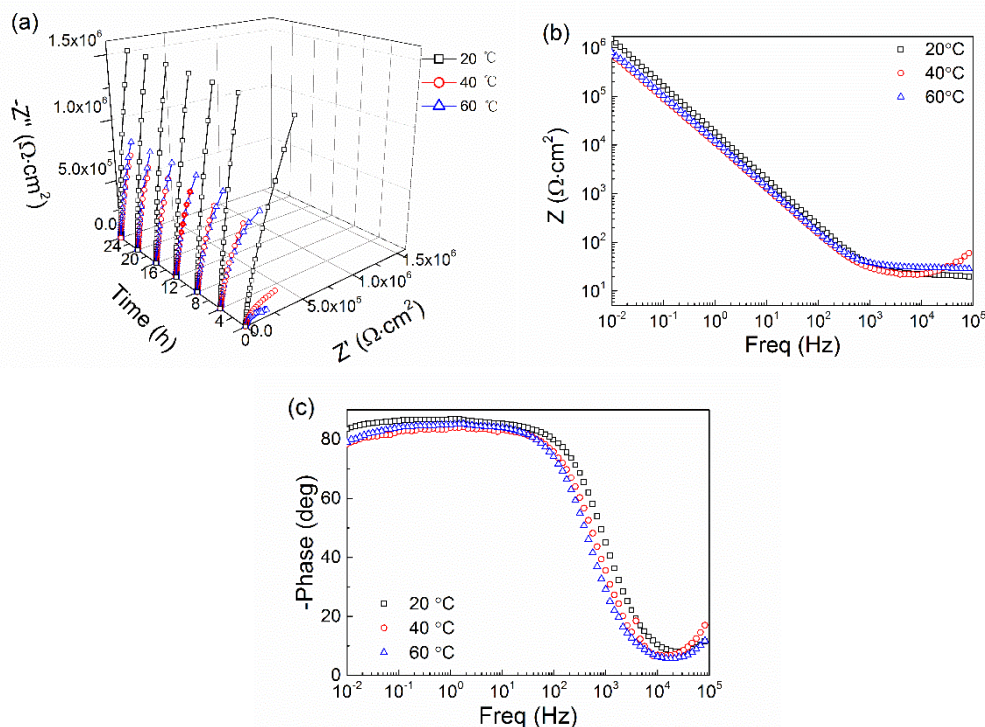
Figure 9. EIS of Zr-based amorphous at OCP in different temperature H_2SO_4 solutions open to air, (a) Nyquist plots, (b) log Z plots at 24th hours, (c) Bode phase angle at 24th hours.
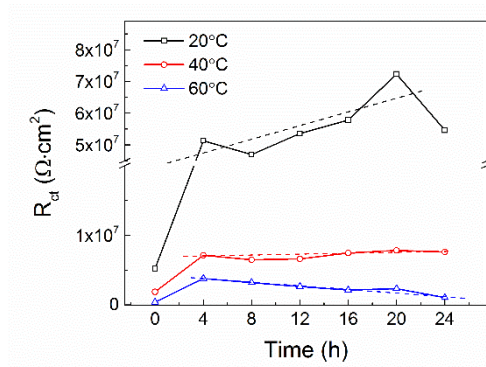
Figure 10. R_{ct} vs. time correlative curves of Zr-based amorphous at OCP in different temperature H_2SO_4 open to air.

The Mott-Schottky curves were obtained at different temperatures, as shown in Fig. 11. It shows that the increase in temperature does not change the passive film type. The calculated acceptor (donor) densities (N_A (N_D)) for the passive films formed on Zr-based BMG at various temperatures are shown in Table 5. The results imply that N_A and N_D of the passive films increase when the passive films are formed in higher temperature acid solutions, indicating that the passive film formed in a higher temperature has a more impurity density. The flat band potentials (E_{fb}) are very close in the solutions at different temperatures, indicating the formation of the same passive layer on the surface of Zr-based BMG.
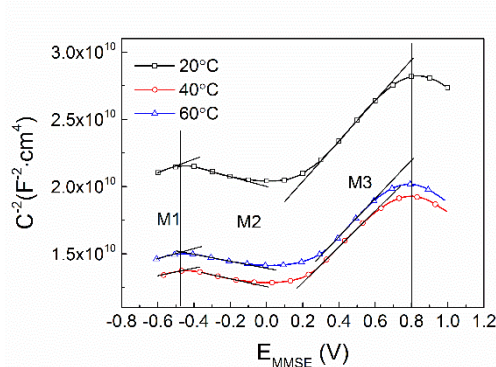
Figure 11. Mott-Schottky curves of formed passive films of the Zr-based BMG in different temperature H_2SO_4 solutions open to air.

Table 5. Mott-Schottky parameters of passive films on Zr-based BMG

T (℃)	n-Type (-0.6;-0.35 V)		p-Type (-0.2;0.2 V)		n-Type (0.3;0.9 V)	
	$N_D(cm^{-3})\times10^{-21}$	E_{fb} (V)	$N_A(cm^{-3})\times10^{-21}$	E_{fb} (V)	$N_D(cm^{-3})\times10^{-21}$	E_{fb} (V)
20	2.25	-4.8	3.10	5.5	0.75	-1.2
40	4.03	-5.4	3.85	4.3	0.85	-0.8
60	3.12	-4.6	4.35	5.4	0.80	-0.8

3.4 Influences of heat treatment temperature on passivation behavior

Fig. 12a shows polarization results of Zr-based BMG of different states in H_2SO_4 solutions. The polarization curves show that the corrosion potential and corrosion current density are very similar to the different heat treatments. Both the corrosion current densities and the corrosion potentials only increase slightly after heat-treatments as the trans-passivation potentials decrease a little (approximate 100 mV). The heat treatment performed at the temperatures lower than T_g does not have obvious effect on the passivation property of $Zr_{60}Cu_{20}Ni_8Al_7Hf_3Ti_2$ BMG in sulfuric acid solution at room temperature.
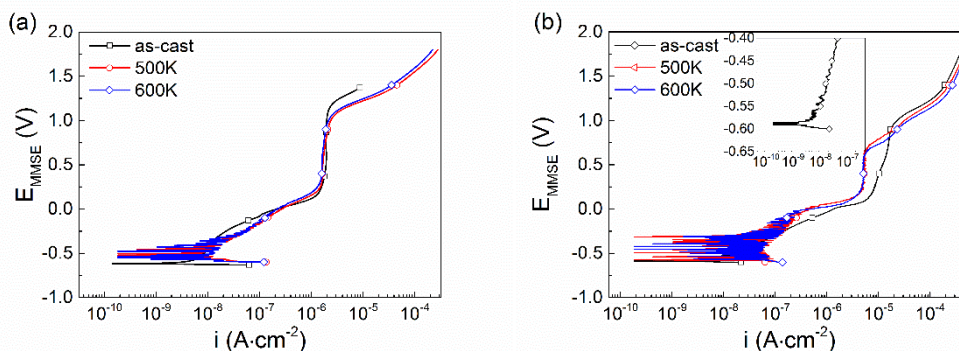

Figure 12. (a) Potentiodynamic polarization curves results of Zr-based metallic glasses in 0.0100 mol· dm^{-3} H_2SO_4 solution at 25 °C and (b) potentiodynamic polarization curves results of Zr-based metallic glass in H_2SO_4 solutions with SiO_2 particles at 25°C.

X.L. Ji et al. have shown that the heat treatment greatly impacts the erosion-corrosion resistance of BMGs [32]. Under high impingement angle, high impact velocity, and high sand concentration, annealed BMG sample treated at highest temperature exhibits the best erosion-corrosion wear resistance in all of the as-cast and annealed BMG samples. It must be emphasized that the heat treatments conducted in this study caused the crystallization of amorphous alloy and all the annealed crystal samples showed lower micro-hardness than as-cast sample [32]. The phases microstructure is totally different when the annealing temperature is lower than T_g. There is not a simple linear dependency between erosion-corrosion resistance and heat treatment temperature.

In this study we performed heat treatments of low temperature and samples maintain amorphous structure after the heat treatments. The erosion-corrosion resistance of the as-cast and annealed Zr-based BMG samples is compared. Fig. 12b shows the polarization curves. Compared with the results obtained in H_2SO_4 solution without slurry, all the as-cast and annealed samples show very close corrosion potential and similar passivation potential, in term of higher corrosion current and higher passivation current. Moreover, the stable passivation region is smaller in erosion-corrosion condition. The most important difference between the as-cast and annealed samples is that the passivation current of annealed Zr-based BMG samples is much lower than that of as-cast sample. The improvement of erosion-corrosion resistance may be attributed to the increase of the micro-hardness (Fig. 13) brought about by the heat treatment. Micro-hardness of BMG samples shows a small quantity of increase, from 440 Hv to 480 Hv after heat treatment. The performed heat treatment temperatures are lower than T_g, and they do not bring about phase transitions, however it causes higher micro-hardness of treated samples. This result is consistent with the findings of Z.H. Zhang et al [33]. Their investigation showed that the structure relaxation caused by annealing at the temperature lower than glass translation temperature T_g makes the micro-hardness increase slowly, and the crystallization caused by annealing at the temperature higher than T_g makes the micro-hardness increase rapidly. Higher micro-hardness of Zr-based metallic glasses results in stronger erosion-corrosion resistance.
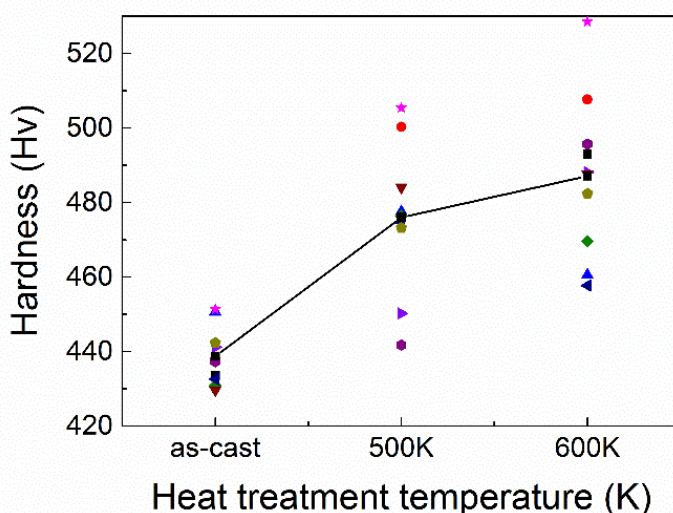
Figure 13. Hardness of Zr-based BMG with different heat treatment.

4. CONCLUSIONS

$Zr_{60}Cu_{20}Ni_8Al_7Hf_3Ti_2$ BMG shows very high stability in different conditions (temperature and concentration) of H_2SO_4 solutions open to air. The corrosion resistance of this BMG is very good in H_2SO_4 solutions when the concentration is less than 1 mol·dm^{-3} and the temperature is below 60 ℃, because $Zr_{60}Cu_{20}Ni_8Al_7Hf_3Ti_2$ BMG possesses spontaneous passivation and a wide passivate potential range. The formed passive films exhibit n-type semiconductor behavior in diverse H_2SO_4 solutions in the passivation potential region and p-type behavior at the transpassivation potential. The order of magnitude of the donor density (N_D) and acceptor density (N_A) of the passive films is comparatively similar in all tested conditions, illustrating that stable dielectric passive films are formed on the amorphous alloy surface.

XPS results show that the passive films have a high content of Al element (38%) which is much higher than the content (8%) in the alloy substrate. In contrast, other elements in the passive films are less than in the alloy substrate. The alloy surface containing more Al_2O_3 and less Cu exhibits better corrosion resistance.

Heat treatment at temperatures lower than T_g does not have obvious effects on the passivation behavior of Zr-based metallic glasses in sulfuric solutions. While in H_2SO_4-sand slurry, the addition of SiO_2 deteriorates the passivation ability of Zr-based metallic glasses, especially for as-cast samples. The heat treatment which does not bring about phase transitions could improve the micro-hardness of Zr-based metallic glasses, and hence results in stronger erosion-corrosion resistance.

References

1. M. Chen, *NPG Asia Mater.*, 3(2011)82.
2. M. M. Trexler and N. N. Thadhani, *Prog. Mater. Sci.*, 55(2010)759.
3. J. Z. Jiang, D. Hofmann, D. J. Jarvis, and H. J. Fecht, *Adv. Eng. Mater.*, 17(2015)761.
4. J. Schroers, *Adv. Mater.*, 22(2010)1566.
5. J.L. Tang, L.S. Yu, J.C. Qiao, Y.Y. Wang, H. Wang, M. Duan, and M. Chamas, *Electrochim. Acta*, 267 (2018)222.
6. A. Tauseef, N. H. Tariq, J. I. Akhter, B. A. Hasan, and M. Mehmood, *J. Alloys Compd.*, 489(2010)596.
7. C. Suryanarayana and A. Inoue, *Int. Mater. Rev.*, 58(2013)131.
8. M. S. Dambatta, S. Izman, B. Yahaya, J. Y. Lim, and D. Kurniawan, *J. Non. Cryst. Solids*, 426 (2015)110.
9. J.C. Qiao, Y.Yao, J.M. Pelletier, and L.M. Keer, *Int. J. .Plast.*, 82(2016)62.
10. J.J. Oak, D. V Louzguine-Luzgin, and A. Inoue, *J. Mater. Res.*, 22(2007)1346.
11. H. B. Lu, L. C. Zhang, A. Gebert, and L. Schultz, *J. Alloys Compd.*, 462(2008)60.
12. N. B. Hua, R. Li, J. F. Wang, and T. Zhang, *Sci. China Phys. Mech. Astron.*, 55(2012)1664.

13. L. Huang, G. Wang, D. Qiao, P. K. Liaw, S. Pang, J. Wang, and T. Zhang, *J. Alloys Compd.*, 504(2010)S159.
14. L. Huang, D. Qiao, B. A. Green, P. K. Liaw, J. Wang, S. Pang, and T. Zhang, *Intermetallics*, 17(2009)195.
15. L.S. Yu, J.L. Tang, J.C. Qiao, H. Wang, Y. Y. Wang, M. Apreutesei, M. Chamas, and M. Duan, *Int. J. Electrochem. Sci.*, 12(2017)6506.
16. Y. Z. Liu, X. T. Zu, C. Li, S. Y. Qiu, X. Q. Huang, and L. M. Wang, *Corros. Sci.*, 49(2007)1069.
17. K. Mondal, B. S. Murty, and U. K. Chatterjee, *Corros. Sci.*, 48(2006)2212.
18. A. Dhawan, S. Roychowdhury, P. K. De, and S. K. Sharma, *J. Non. Cryst. Solids*, 351(2005)951.
19. U. K. Mudali, S. Baunack, J. Eckert, L. Schultz, and A. Gebert, *J. Alloys Compd.*, 377(2004)290.
20. L. Liu, C. L. Qiu, H. Zou, and K. C. Chan, *J. Alloys Compd.*, 399(2005)144.
21. C. Li, D. Chen, W. Chen, L. Wang, and D. Luo, *Corros. Sci.*, 84(2014)96.
22. V. B. Singh and A. Gupta, *Mater. Chem. and Phys.*, 85(2004)12.
23. H. O. Gulsoy, S. Pazarlioglu, N. Gulsoy, B. Gundede, and O. Mutlu, *J. Mech. Behav. Biomed. Mater.*, 51(2015)215.
24. M. Kaseem, Y. H. Lee, and Y. G. Ko, *Mater. Lett.*, 182(2016)260.
25. W.J. Ge, B.Y. Li, E. Axinte, Z. T. Zhang, C. Y. Shang, and Y. Wang, *Miner. Met. & Mater. Soc.*, 69(2017)776.
26. R. N. Mutlu, B. D. Mert, S. Ateş, S. Gündüz, and B. Yazıcı, *Prot. Met. Phys. Chem. Surfaces*, 53(2017)733.
27. L. L. Wang, W. Wang, Y. L. Fan, X. X. Qi, J. H. Liu, and Z. Y. Zhang, *Trans. Nonferrous Met. Soc. China (English Ed.)*, 27(2017)1551.
28. Z. Feng, X. Cheng, C. Dong, L. Xu, and X. Li, *Corros. Sci.*, 52(2010)3646.
29. J. Bisquert, G. Garcia-Belmonte, and F. Fabregat-Santiago, *J. Solid State Electrochem.*, 3(1999)337.
30. H. J. Jang and H. S. Kwon, *J. Solid State Electrochem.*, 19(2015)3427.
31. Ž. Petrović, N. Lajçi, M. Metikoš-Huković, and R. Babić, *J. Solid State Electrochem.*, 15(2011)1201.
32. X. Ji, Y. Shan, Y. Chen, and H. Wang, *J. Mater. Eng. Perform.*, 25(2016)2340.
33. Z. Zhang and J. Xie, *Mater. Sci. Eng. Ab*, 407(2005)161.